Acta Pharmaceutica Sinica B 2021;11(2):520–533

Chinese Pharmaceutical Association
Institute of Materia Medica, Chinese Academy of Medical Sciences

Acta Pharmaceutica Sinica B

www.elsevier.com/locate/apsb
www.sciencedirect.com

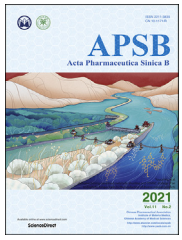

ORIGINAL ARTICLE

pH-sensitive and bubble-generating mesoporous silica-based nanoparticles for enhanced tumor combination therapy

Zhiming Zhang[†], Chenlu Huang[†], Li Zhang, Qing Guo, Yu Qin, Fan Fan, Boxuan Li, Bao Xiao, Dunwan Zhu[*], Linhua Zhang[*]

Tianjin Key Laboratory of Biomedical Materials, Key Laboratory of Biomaterials and Nanotechnology for Cancer Immunotherapy, Institute of Biomedical Engineering, Chinese Academy of Medical Sciences & Peking Union Medical College, Tianjin 300192, China

Received 16 April 2020; received in revised form 28 June 2020; accepted 24 July 2020

KEY WORDS

Mesoporous silica;
pH-sensitive;
Bubble-generating;
Targeting modification;
Combination therapy

Abstract Chemotherapy has been a major option in clinic treatment of malignant tumors. However, single chemotherapy faces some drawbacks, such as multidrug resistance, severe side effects, which hinder its clinic application in tumor treatment. Multifunctional nanoparticles loading with chemotherapeutic agent and photosensitizer could be a promising way to efficiently conduct tumor combination therapy. In the current study, a novel pH-sensitive and bubble-generating mesoporous silica-based drug delivery system (denoted as M(a)D@PI-PEG-RGD) was constructed. Ammonium bicarbonate (NH_4HCO_3; abc) and chemotherapeutic agent doxorubicin (DOX) were loaded into the pores of mesoporous silica. Indocyanine green (ICG) as a photothermal and photodynamic agent was loaded onto the polydopamine (PDA) layer surface. The synthesized nanoparticles displayed a narrow polydispersity (PDI) and small particle size as characterized through dynamic light scattering-autosizer analysis. The nanoparticles also showed high targeting efficacy through RGD modification as indicated by cellular uptake and animal studies. DOX release analysis confirmed that the nanoparticles were pH-dependent and that NH_4HCO_3 accelerated drug release. At the same time, the nanoparticles had obvious photothermal and photodynamic effects performed by ICG which restrained tumor growth remarkably. In summary, the multifunctional nanoparticles presented a promising system for combination therapy.

*Corresponding authors.
E-mail addresses: zhudunwan@bme.pumc.edu.cn (Dunwan Zhu), zhanglinhua@bme.pumc.edu.cn (Linhua Zhang).
[†]These authors made equal contributions to this work.

Peer review under responsibility of Chinese Pharmaceutical Association and Institute of Materia Medica, Chinese Academy of Medical Sciences.

https://doi.org/10.1016/j.apsb.2020.08.013

1. Introduction

Malignant tumor has been the secondary cause of death after cardiovascular and cerebrovascular diseases. Chemotherapy, as the most used treatment in clinic, achieves limited therapeutic outcome owing to the serious side effects and short blood circulation time of chemotherapeutic drugs[1−3]. For instance, doxorubicin (DOX) can restrain DNA and RNA synthesis and kill tumor cells effectively, which has become a common type of drug for treating cancer[4−6]. However, this kind of drug can cause serious side effects, especially on heart function. In recent years, nanocarriers have attracted much attention due to their excellent biochemical properties and great potentials in the diagnosis and treatment of tumors. Nanocarriers can prolong the duration of drug circulation and avoid premature excretion by the kidneys. In addition, anti-tumor drugs would be delivered to tumor sites through enhanced permeability and retention (EPR) and targeting effect after loaded into nanocarriers. Chemotherapy based on nanoparticles has continuous effects and can treat both primary and metastatic tumors which enable chemotherapy to be widely applied in anti-tumor research.

Mesoporous silica nanoparticles (MSNs) is a new generation of inorganic drug-delivery system and display great potentials in biomedical application resulting from large pore volume and high surface area as well as outstanding biocompatibility[7,8]. In general, supramolecular assemblies of surfactants play an indispensable role in synthesis of MSNs, which could self-aggregate into micelles and then the silica precursors would form an inorganic–organic hybrid material at the surface of micelles. At last, solvent extraction and calcination are utilized to remove template surfactant in order to generate pores[9]. In our study, DOX was loaded with MSNs in order to perform chemotherapy, and NH_4HCO_3 was also encapsulated into the pores of MSNs. Recent research has demonstrated that NH_4HCO_3 can decompose into CO_2 bubbles, NH_3, and H_2O in acidic environment and heating condition[10−12], which may accelerate the release of drugs and enhance the effect of chemotherapy. Moreover, the properties of MSNs can be enhanced through surface modifications with polymers or small molecules such as polydopamine (PDA) and folic acid. PDA is a biomimetic polymer that can manufacture many types of materials containing copolymers, ceramics, and semiconductors utilized by oxidative polymerization under weak base conditions (at pH value of 8.0−8.5)[13]. It has been widely developed as the drug delivery carrier and is able to form an adhesive layer on the surface of MSNs[14−16]. To prevent DOX leakage from MSNs, we introduced PDA to coat MSNs. Moreover, PDA is a pH-sensitive polymer, and the PDA layer can be destroyed in acidic conditions. This property makes drug release from MSNs, as the nanoparticles accumulate at tumor sites where the pH value typically remains below 7.4[17].

Although chemotherapy based on nanoparticles owns unique advantages for primary and metastatic tumors, its clinical application has still been limited due to the complexity, diversity, heterogeneity as well as multi-drug resistance of tumors. Over recent years, photodynamic therapy (PDT) as well as photothermal therapy (PTT) has been increasingly recognized as the potential means to treat cancer due to their treatment accuracy and minimal damage for normal cells and tissues[18,19]. With photosensitizing agents, PTT can generate local hyperthermia under irradiation of near-infrared (NIR) laser, which can further enhance treatment efficacy and reduce side effect[20]. Some photosensitizing agents are also able to produce reactive oxygen species (ROS) if irradiated with NIR laser. ROS is a kind of short-lived compound that can lead to DNA damage and cell apoptosis; thus, photodynamic effect can be utilized to kill tumor cells[21−23]. Indocyanine green (ICG) is approved by U.S. Food and Drug Administration (FDA) as a kind of tricarbocyanine dye, which absorbs NIR laser with a wavelength of 808 nm, generates ROS, and emits heat[24]. Therefore, ICG is a suitable type of photosensitizing agent to realize combination therapy of PTT and PDT resulting from these characterizations. However, some studies indicate that PDT and PTT are only able to kill primary tumors but cannot treat metastatic tumors thoroughly and these therapies are suffering from several drawbacks related to limited laser penetration in tumor tissues. In recent years, combination therapy has been widely studied and can achieve synergistic therapeutic effects which are theoretically stronger than every component therapy. In the current study, this combination therapy containing chemotherapy, PTT, and PDT to treat cancer were investigated.

Targeting modification can improve the efficiency of tumor cell uptake and reduce side effects of antitumor drugs. In previous studies, the surfaces of nanoparticles have usually been modified with small ligands, such as peptides, antibody, vitamin, polysaccharide, and so on[25−28]. RGD is a kind of short peptide and widely studied[29−33]. As a ligand of integrin recognition site, RGD displays great adhesion capacity between extracellular matrix cells and cells[34]. In our study, RGD was used to modify nanoparticles and enhance therapeutic effects of anticancer drugs.

In this work, pH-sensitive and bubble-generating mesoporous silica-based nanoparticles were constructed to enhance tumor combination therapy. DOX and NH_4HCO_3 were loaded into MSNs pores by diffusion, and MSNs was coated with PDA layer, which was pH-sensitive and can control the profile of the drug release. And then ICG as a photothermal and photodynamic agent was loaded onto the PDA layer surface. The nanoparticles were also modified with polyethylene glycol (PEG) as well as RGD to improve the stability and accuracy. Under NIR irradiation, the nanoparticles can generate ROS and induce temperature increase performed by ICG. In addition, acidic environment and high temperature also enable NH_4HCO_3 to discompose and thus accelerate DOX release (as shown in Scheme 1). Overall, the multifunctional pH-sensitive and bubble-generating mesoporous silica-based nanoparticles will provide a novel strategy to improve the chemotherapy, PDT and PTT in order to enhance the therapeutic effect of tumor treatment.

2. Materials and methods

2.1. Materials

Doxorubicin hydrochloride was obtained from Dalian Biological Co., Ltd. (Dalian, China). Indocyanine green (ICG), dopamine hydrochloride, *N*-(3-dimethylaminopropyl)-*N′*-ethylcarbodiimide hydrochloride (EDC), *N*-hydroxysuccinimide (NHS), 1,3-diphenylisobenzofuran (DPBF), hoechst, *in situ* cell detection kit, pod, and 2′,7′-dichlorofluorescin diacetate (DCFH-DA) were all obtained from Sigma−Aldrich (ST. Louis, MO, USA). Ammonium bicarbonate (NH_4HCO_3; abc) was purchased from Tianjin Jiang Tian Chemical Technology Co., Ltd. (Tianjin, China). Tetraethyl orthosilicate (TEOS), hexadecyl trimethyl ammonium bromide (CTAB), tri (2-carboxyethyl) phosphine hydrochloride (TCEP) and ammonium fluoride (NH_4F) were obtained from Shanghai Aladdin Bio-chem Technology Co., Ltd.

(Shanghai, China). SH-PEG_{2000} and SH-PEG_{2000}-COOH were obtained from Shanghai Peng Sheng Biological Co., Ltd. (Shanghai, China). Cyclo (RGDyK) was purchased from China Peptides Co., Ltd. (Shanghai, China). One solution cell proliferation assay (MTS) was purchased from Promega (Madison, WI, USA). Mounting medium, antifading (with DAPI) was obtained from Solarbio life sciences Co., Ltd. (Beijing, China). Carboxy-H_2DCFDA was obtained from Life Technologies Corporation (Eugene, OR, USA).

2.2. Preparation of M(a)

Briefly, 3 g NH_4F and 1.82 g CTAB were dispersed in 480 mL distilled water and heated in oil bath (DF-101S, Gongyi Yu Hua instrument and Equipment Co., Ltd., Zhengzhou, China). When the temperature rose to 80 °C, 9 mL TEOS was added into the mixture dropwise. Then, the mixture solution was stirred vigorously for 6 h.

After stirring, the product was separated by centrifugation (13,000 rpm, 10 min, 3K15, Sigma Laborzentrifugen GmbH, Osterode am Harz, Germany) and washed with distilled water and ethyl alcohol several times. To remove redundant CTAB, the product was added into 400 mL ethyl alcohol with 8 mL hydrochloric acid before being refluxed for 24 h at 80 °C (Gongyi Yu Hua instrument and Equipment Co., Ltd.). The procedure was repeated twice to remove CTAB thoroughly.

For loading NH_4HCO_3, 30 mg MSNs were added into 2 mL of NH_4HCO_3 solution (2 mol/L) and stirred vigorously for 6 h at room temperature. Then the product was separated by centrifugation (13,000 rpm, 10 min, Sigma Laborzentrifugen GmbH). Finally, the product was washed with distilled water several times in order to remove excess NH_4HCO_3.

2.3. Preparation of M(a)D@PI

DOX was loaded into the nanoparticles through diffusion. Briefly, 30 mg M(a) was added into 1.5 mL DOX solution (10 mg/mL) and stirred for 24 h at room temperature. The resulting product was collected by centrifugation (13,000 rpm, 10 min, Sigma Laborzentrifugen GmbH) and washed with distilled water several times to remove superficial drugs. To make M(a)D coated with PDA, 15 mg dopamine hydrochloride and 30 mg M(a)D were dispersed in 15 mL Tris-HCl solution (pH 8.5) and stirred for 6 h. After that, the production could be collected by centrifugation (13,000 rpm, 10 min, Sigma Laborzentrifugen GmbH) and washed with distilled water several times.

Briefly, 30 mg M(a)D@P was dispersed in 1.5 mL ICG solution (10 mg/mL) and stirred for 8 h at room temperature. ICG could be absorbed onto PDA surface. Afterwards, the product was collected by same method mentioned above.

2.4. Preparation of M(a)D@PI-PEG and M(a)D@PI-PEG-RGD

SH-PEG_{2000} and SH-PEG_{2000}-COOH were connected to the PDA layer surface *via* Michael addition reaction. To prepare M(a)D@PI-PEG, 30 mg M(a)D@PI, 0.6 mg TCEP and 30 mg SH-PEG_{2000} were added into 15 mL Tris-HCl solution (pH 8.5) and stirred for 6 h. The product could be collected by centrifugation (13,000 rpm, 10 min, Sigma Laborzentrifugen GmbH).

To obtain M(a)D@PI-PEG-RGD, 30 mg M(a)D@PI, 0.6 mg TCEP and 5 mg SH-PEG_{2000}-COOH were added into 15 mL Tris-HCl solution (pH 8.5) and stirred for 1 h. Then 25 mg SH-PEG_{2000} were put into the mixture solution and stirred for another 5 h. The product could be collected by centrifugation (13,000 rpm, 10 min, Sigma Laborzentrifugen GmbH). To modify the nanoparticles with RGD, 30 mg M(a)D@PI-PEG-COOH, 4.79 mg EDC and 5.75 mg NHS were added into water to activate for 15 min. 1.5 mg cyclo (RGDyK) were added into the mixture solution and stirred for 8 h. The product could be collected by centrifugation (13,000 rpm, 10 min, Sigma Laborzentrifugen GmbH).

2.5. Characterization of nanoparticles

The zeta potentials and sizes of nanoparticles were investigated by Malvern Zetasizer (Nano-ZS, Malvern Instruments, Malvern, UK). Different samples were measured with the concentration of 150 μg/mL in distilled water. To analyze long-term stability of nanoparticles, MSNs and M(a)D@PI-PEG-RGD were dispersed in distilled water and measured by Malvern Zetasizer (Malvern Instruments) for 7 days. The drug loading content (LC) was calculated using the following Eq. (1):

$$\mathrm{LC}\,(\%) = \frac{\text{Weight of drugs loaded into nanoparticles}}{\text{Weight of nanoparticles}} \times 100 \qquad (1)$$

DOX loading content of M(a)D was determined by the concentration change of DOX before and after reaction, which can be obtained from the measurement by UV−Vis spectrometry (Lambda 35, PerkinElmer, Walsham, MA, USA) at the wavelength of 480 nm. To determine ICG loading content of M(a)D@PI-PEG-RGD, 1 mg lyophilized M(a)D@PI-PEG-RGD was dispersed in 2 mL DMSO. Then the sample was sonicated (VCX-130 PB, Sonics & Materials, Newtown, CT, USA) for 20 min to ensure that ICG dissolved in DMSO thoroughly. ICG concentration was determined by calibration curve method with UV−Vis spectrometry at the wavelength of 780 nm.

To investigate the morphological characterization of nanoparticles, different formulations [MSNs, M(a)D@P, M(a)D@PI-PEG and M(a)D@PI-PEG + laser with the same concentration, 5 mg/mL, laser: 1 W/cm^2, 5 min] were dispersed with distilled water by sonication (Sonics & Materials). After that, sample suspensions were dropwise added onto the carbon-coated copper grid and then dried for 12 h. Then these samples were observed with transmission electron microscope (JEM-100XII, Hitachi, Tokyo, Japan). To characterize nanoparticles by N_2 adsorption−desorption isotherms, MSNs (500 mg) were degassed in vacuum oven for 24 h with the temperature of 120 °C and then characterized by N_2 adsorption−desorption isotherms (ASAP 2020, Micromeritics, Norcross, GA, USA).

15 mg M(a)D@PI-PEG-RGD was added into phosphate buffer solution (PBS, pH 7.4 and 5.5) to confirm NH_4HCO_3 can generate CO_2 bubbles. ICG and M(a)D@PI-PEG-RGD were dispersed in distilled water (with the same ICG equivalent concentration of 8 μg/mL) and were measured by UV−Vis spectrometry in 7 days in order to analyze the stability of ICG. In order to prove that DOX and ICG were loaded onto nanoparticles successfully, DOX, ICG and M(a)D@PI-PEG-RGD were dispersed in distilled water and were measured by UV−Vis spectrometry. Furthermore, X-ray photoelectron spectroscopy (XPS) was also performed to analyze the structures of nanoparticles (AXIS ULTRA DLD, Kratos, Manchester, UK).

2.6. Photothermal effect of different samples in vitro

To investigate the photothermal effect of nanoparticles *in vitro*, different formulations [H_2O, MSNs, ICG, M(a)D@P, M(a)D@PI, M(a)D@PI-PEG] with the same ICG equivalent concentration (8 μg/mL) were dispersed with distilled water and characterized under the laser irradiation of 808 nm (1 W/cm^2, LS-008, Zhongshan You Sheng Photoelectric Technology Co., Ltd., Zhongshan, China) within 5 min by a digital thermometer (FLIR E6 MXS, FLIR Systems, Werwilson, OR, USA). Furthermore, temperature changes of different concentrations for M(a)D@PI-PEG were also detected. To verify the advantages of nanoparticles, temperature-rise and cool-down processes for M(a)D@PI-PEG and free ICG at the same equivalent concentration of 8 μg/mL were detected within 40 min.

2.7. In vitro photodynamic effect

Nanoparticles loading ICG can induce ROS under laser irradiation. DPBF was utilized to detect the capability of ROS generation with different formulations [DPBF, ICG + DPBF, M(a)D@P + DPBF, M(a)D@PI + DPBF, M(a)D@PI-PEG + DPBF] which were dispersed in *N,N*-dimethylformamide (DMF) with the same ICG equivalent concentration (8 μg/mL) within 5 min under laser irradiation at the wavelength of 808 nm (1 W/cm^2). At the same time, the absorbances of different samples were measured at 410 nm through UV−Vis spectrophotometer (PerkinElmer).

2.8. In vitro drug release

5 mg lyophilized samples [M(a)D@PI-PEG] were dispersed in PBS (1 mL, pH 7.4 and 5.5) and then placed in dialysis bags (MW 3500). Dialysis bags were placed in PBS (20 mL, pH 7.4 and 5.5). Samples were stored at 37 °C with the shaking speed of 150 rpm (HNY-200D, Honour Instrument Co., Ltd., Tianjin, China). To investigate the NIR irradiation effect on drug release, several samples were dispersed in PBS (pH 7.4 and 5.5) and irradiated by laser (808 nm, 1 W/cm^2, 5 min). Finally, these samples were loaded into dialysis bags. At predetermined time, replacing 20 mL incubation solution with fresh PBS. The release profile of DOX was studied by calibration curve method with fluorescence spectrophotometer (Lambda, PerkinElmer, Walsham, MA, USA). We also have evaluated the DOX release profiles of M(a)D. 5 mg nanoparticles were dispersed in PBS (1 mL, pH 7.4 and 5.5) and then placed in dialysis bags. These dialysis bags were placed in 20 mL PBS and stored at 37 °C with the shaking speed of 150 rpm (Honour Instrument Co., Ltd.). Replacing 20 mL incubation solution with fresh PBS at predetermined time. The release profile of DOX was detected by calibration curve method with fluorescence spectrophotometer (PerkinElmer).

2.9. Cell culture

CT26 cells were cultured with RPMI-1640 supplemented containing 1% (*v*/*v*) penicillin/streptomycin and 10% (*v*/*v*) FBS in a common incubation condition (5% CO_2, 37 °C, HERAcell 240i, Thermo Fisher, Walsham, MA, USA).

2.10. In vitro cytotoxicity

The cytotoxicity of CT26 cells samples was tested by MTS assay. Briefly, CT26 cells (4×10^4/mL, 100 μL) were seeded in 96-well plates and then incubated for 24 h. Different formulations [DOX, M(a)D@P-PEG, M(a)D@P-PEG-RGD] with different DOX equivalent concentrations (8, 4, 2, 1 and 0.5 μg/mL, respectively) were then added to plates and incubated for 48 and 72 h. Afterwards, CT26 cells were incubated with MTS solution containing RPMI-1640 supplemented (20 μL MTS solution, 100 μL RPMI-1640 supplemented/well) for 30 min. At last, the absorbance value of each well was evaluated by Varioskan Flash spectral scanning multimode reader (Thermo Varioskan, Thermo Fisher, Walsham, MA, USA) at 490 nm.

To investigate the photothermal and photodynamic effect of free ICG and nanoparticles, different formulations [ICG, M(a)@PI-PEG, M(a)@PI-PEG-RGD] with the same ICG equivalent concentration (8 and 4 μg/mL, respectively) were then added to plates. The NIR irradiation (1 W/cm^2, 5 min, Zhongshan You Sheng Photoelectric Technology Co., Ltd.) was given after 4 h of adding formulations and then cells were cultured for another 20 h. Afterwards, cells were dealt with the same method mentioned above.

The cytotoxicity of MSNs, M(a)@P-PEG, M@P-PEG, M(a)@PI-PEG, M(a)@PI-PEG-RGD was also evaluated in the study. Briefly, different formulations were added into plates and cultured for 72 h. Finally, cells were dealt with the same method mentioned above.

2.11. Cellular uptake experiment in vitro

To explore *in vitro* cellular uptake, CT26 cells were seeded in the confocal dishes at the density of 4×10^4/well and incubated for 24 h. Different formulations [DOX + ICG, M(a)D@PI-PEG, M(a)D@PI-PEG-RGD] with the equivalent DOX concentration (8 μg/mL) and equivalent ICG concentration (1.36 μg/mL) were then added to dishes and incubated for 3 h. Laser (1 W/cm^2, 5 min, 808 nm) was given after 2 h of adding different formulations. Then these cells were washed twice by fresh PBS and fixed with 4% paraformaldehyde for 10 min. Then cells were washed twice by PBS and incubated with Hoechst (8 μg/mL) for 5 min. Finally, cells were washed twice by PBS before being observed with CLSM (confocal laser scanning microscopy, LSM710, Carl Zeiss, Jena, Germany).

We also used flow cytometry (BD FACS Calibur, BD Biosciences, San Jose, CA, USA) to analyze cellular uptake quantitatively. CT26 cells were seeded at the density of 4×10^5/well in 24-well plates. After 24 h, added different formulations into plates and incubated for 3 h 808 nm laser (1 W/cm^2, 5 min) was given after 2 h of adding different formulations. Cells were detached by tryple solution (80% PBS, 20% tryple, *v*/*v*) and washed twice with PBS before detected by flow cytometer (BD Biosciences).

For competitive binding experiments, CT26 cells were pretreated with free RGD for 3 h before the addition of M(a)D@PI-PEG-RGD. Then these cells were cultured for 3 h. The other group was treated with M(a)D@PI-PEG-RGD (with the same equivalent concentration of DOX, 8 μg/mL) directly for 3 h. These cells were washed twice by fresh PBS and fixed with 4% paraformaldehyde for 10 min. Then cells were washed twice by PBS and incubated with Hoechst (8 μg/mL) for 5 min. Finally, cells were washed twice by PBS before being observed with CLSM (Carl Zeiss).

2.12. In vitro ROS detection

CT26 cells with the density of 4×10^5/well were seeded in the confocal dishes for 24 h. And then, cells were incubated with different formulations [DOX + ICG, M(a)D@PI-PEG, M(a)D@PI-

PEG-RGD] with the same equivalent DOX concentration (8 μg/mL) and equivalent ICG concentration (1.36 μg/mL) for 3 h. After that, cells were washed twice by PBS and incubated with carboxy-H_2DCFDA (6 μg/mL) for 15 min. Cells were then washed twice by PBS and given NIR irradiation (808 nm, 1 W/cm^2, 5 min). These cells were fixed with 4% paraformaldehyde for 10 min. At last, cells were washed twice by fresh PBS and incubated with Hoechst (8 μg/mL) for 5 min. Cells were washed twice by PBS before being observed under CLSM.

In order to analyze quantitatively with flow cytometry (BD Biosciences), cells were seeded at the density of 4×10^5/well in 24-well plates. After 24 h, these cells were incubated with different formulations for 3 h. Then cells were washed twice with PBS and incubated with carboxy-H_2DCFDA (6 μg/mL) for 15 min. Then washed cells twice with PBS and treated cells with NIR irradiation (808 nm, 1 W/cm^2, 5 min). Cells were detached by tryple solution (80% PBS, 20% tryple, *v/v*) and were washed twice with PBS before detected by flow cytometer (BD Biosciences).

2.13. Tumor models

All 6−8 weeks BALB/c female mice were obtained from SPF (Beijing) Biotechnology Limited Company. The study was conducted in accordance with guidelines and ethics of Chinese Academy of Medical Science and Peking Union Medical College. Each mouse was injected with 2×10^6 CT26 cells in saline (100 μL) in the right flank. Tumor volume could be calculated as the following Eq. (2):

$$\text{Tumor volume} = \text{Tumor length} \times \text{Tumor width}^2/2 \quad (2)$$

when tumor volume of each mouse reached around 100 mm^3, animal studies started.

2.14. Imaging in vivo and biodistribution research

The mice for images *in vivo* and biodistribution assay were divided randomly into 3 groups. Different formulations [DOX + ICG, M(a)D@PI-PEG, M(a)D@PI-PEG-RGD with same equivalent DOX and ICG concentration, DOX 8, ICG 1.36 mg/kg] were injected *via* tails. Near-infrared fluorescence images were collected after 12, 24, 48 and 72 h of injection by the Imaging System *in vivo* (CRI Maestro, CRi Maestro™, Cambridge, MA, USA). Some mice were executed after 12 h of injection to obtain *ex vivo* images of hearts, livers, spleens, lungs, kidneys and tumors.

To analysis the distribution of M(a)D@PI-PEG-RGD in organs, mice were injected intravenously with nanoparticles. After injection, these mice were executed at 12 and 72 h. After that, hearts, livers, spleens, lungs, kidneys and tumors from different mice were collected, weighed and then digested with nitric acid and hydrochloric acid (1:3, *v/v*). These different samples were analyzed with inductively coupled plasma mass spectrometry (ICP-MS, iCAP™ RQ, Thermo Fisher, Walsham, MA, USA).

2.15. In vivo photothermal effect

The mice for photothermal effect assay were divided randomly into 5 groups. Different formulations [PBS, DOX + ICG, M(a)D@PI-PEG, M(a)D@PI-PEG-RGD, M(a)D@P-PEG-RGD with same equivalent DOX and ICG concentration, DOX 8 mg/kg, ICG 1.36 mg/kg] were injected *via* tails. After 12 h, tumor sites of different groups were dealt with NIR irradiations (808 nm, 1 W/cm^2) and temperature changes of different groups were detected within 5 min by a digital thermometer. Images of max temperatures were recorded by an IR camera (FLIR E6 MXS, FLIR Systems).

2.16. In vivo ROS detection

The mice for *in vivo* ROS detection were divided randomly into 4 groups. Different formulations [PBS, DOX + ICG, M(a)D@PI-PEG, M(a)D@PI-PEG-RGD with same equivalent DOX and ICG concentration, DOX 8 mg/kg and ICG 1.36 mg/kg] were injected *via* tails. These mice were intratumorally injected with DCFH-DA (2.5 mg/kg) after 10 h of injection. 808 nm laser irradiations were given after 2 h. These mice were executed and then tumors were fixed, dehydrated and cut into slices. Finally, slices were dealt with antifade mounting medium containing DAPI and observed under CLSM.

2.17. Tunnel apoptotic cell detection of tumor tissues

The mice were divided into 4 groups randomly. Different formulations [PBS, DOX + ICG, M(a)D@PI-PEG, M(a)D@PI-PEG-RGD with same equivalent DOX and ICG concentration, DOX 8 mg/kg and ICG 1.36 mg/kg] were intravenously injected into mice *via* tails. 808 nm laser irradiations were given after 12 h. Then these mice were executed. The tumor sites of the mice were stored in 4% paraformaldehyde and dehydrated, and then cut into slices. Finally, these slices were dealt with *in situ* cell detection kit and antifade mounting medium containing DAPI and then observed *via* CLSM. Tunnel apoptotic cell detection of tumor tissues was completed to analyze the efficiency of antitumor.

2.18. In vivo antitumor efficiency

In order to analyze antitumor capability, different formulations [PBS, DOX + ICG, M(a)D@PI-PEG, M(a)D@PI-PEG-RGD with same equivalent DOX and ICG concentration, DOX 8 mg/kg and ICG 1.36 mg/kg] were intravenously injected 3 times into mice *via* tails over 4 days. Laser irradiations (808 nm, 1 W/cm^2, 5 min) were given after 12 h. The volume of tumor and body weight of every mouse were measured ever two days. The experiment lasted 14 days. At the end of animal experiment, these mice were executed and these major organs containing hearts, livers, spleen, lungs as well as kidneys were collected and stored in 4% paraformaldehyde and dehydrated, cut into slices. Hematoxylin and eosin (H&E) were employed to evaluate changes of the major organs after experiment.

2.19. Statistical analysis

Data was showed as mean ± SD and the differences amongst groups were determined by One-way ANOVA method. $^*P < 0.05$ and $^{**}P < 0.01$ represent statistical significance.

3. Results and discussion

3.1. Characterizations of nanoparticles

The size, polydispersity (PDI) and zeta potential of the nanoparticles are shown in Table 1. It indicates that sizes of nanoparticles range from 160 to 300 nm. The sizes of nanoparticles are small enough to circulate in blood and can be taken up by cells through endocytosis[35].

PDI are acceptable and demonstrates that sizes of nanoparticles are relatively homogeneous. The stability of nanoparticles can be essentially reflected by the Zeta potential. Since the negative charge of MSNs was partially neutralized by the positive charge of DOX, the zeta potential of M(a)D (-18.93 ± 0.19 mV) increased compared with that of MSNs (-24.40 ± 0.28 mV). After being coated with PDA and absorbing ICG, zeta potential of M(a)D@PI (-26.60 ± 0.22 mV) decreased. Meanwhile, the sizes of nanoparticles increased significantly after being modified with PEG and RGD. It confirms that PEG and RGD were connected to the surface of nanoparticles successfully due to the changes of sizes and zeta potentials. From Supporting Information Fig. S1A, the result indicates that changes of nanoparticles sizes were not obvious and nanoparticles were stable within 7 days. The drug-loading content was determined by calibration curve method. The DOX loading content of M(a)D is $7.29 \pm 0.28\%$. The ICG loading content of M(a)D@PI-PEG-RGD is $1.24 \pm 0.2\%$. MSNs were spherical in appearance and relative uniform in size, pores of MSNs can be observed clearly which can be seen from Supporting Information Fig. S2A. After coated with PDA, the PDA layer can also be observed clearly (Figs. S2C and S2D). N_2 adsorption−desorption isotherms and BJH adsorption curve are shown as Fig. S2B. The results indicate the nanoparticles were mesoporous materials and pore size distribution was relatively uniform. The BET surface area of MSNs is 70.82 m^2/g. BJH cumulative volume of pores between 1.7 and 300.0 nm width is 0.25 cm^3/g.

After adding M(a)D@PI-PEG-RGD into PBS (pH 7.4 and 5.5), nanoparticles can generate CO_2 bubbles under acidic condition while there was no similar phenomenon observed in PBS (pH 7.4, Fig. S1B). In addition, Supporting Information Fig. S3 also proves PDA layer could be destroyed under laser irradiation due to the generation of CO_2 bubbles. UV−Vis spectrometry of M(a)D@PI-PEG-RGD and ICG are compared in Figs. S1C and 1D. For M(a)D@I-PEG-RGD, a strong absorption peak of 800 nm can still be observed on Day 7 compared with free ICG, indicating that the stability of ICG was able to be enhanced by being loading onto PDA layer. According to Supporting Information Fig. S4, absorption peaks of ICG and DOX could be observed from nanoparticles, indicating the nanoparticles have loaded DOX and ICG successfully. Furthermore, XPS was performed to analyze the structures of nanoparticles (Supporting Information Fig. S5). Only MSNs contained silicon atoms, while PDA, PEG and RGD did not. For silicon peaks (Si2p), the lower intensity of M@P, M@P-PEG and M@P-PEG-RGD could prove that MSNs have been modified with PDA, PEG and RGD successfully. Besides, the intensity of Si2p for M@P-PEG-RGD was slightly lower than that for M@P-PEG, which resulted from incorporation of RGD.

3.2. *Photothermal effect and photodynamic effect evaluation in vitro*

To analyze photothermal effect of nanoparticles, an IR camera (FLIR Systems) was utilized to record temperature change. Free ICG easily suffers from serious photo-bleaching under NIR irradiation and cannot exist for a long time[36]. It is necessary to introduce nano-system to enhance stability of ICG. Temperature changes of M(a)D@PI-PEG became more obvious with the increase of concentration for ICG equivalent concertation according to Fig. 1A. It was significant that M(a)D@PI-PEG had more effective photothermal effect compared with free ICG and M(a)D@P *in vitro*. The nanoparticles under laser irradiation will cause irreversible damage to tumor tissues. H_2O displayed no photothermal effect (Fig. 1B). We also further analyzed the photothermal effect of M(a)D@PI-PEG and free ICG. It was found that the changes of the temperature for M(a)D@PI-PEG were still significant during 4 cycles of temperature-rise and cool-down process which is shown as Fig. 1C. The obvious photobleaching of ICG was also observed. After 4 cycles, ICG can no longer induce temperature change significantly. These results indicate that M(a)D@PI-PEG had remarkable photothermal effect. ICG loaded onto nanoparticles was more stable than free ICG.

Table 1 Characterization of nanoparticles.

Sample	Size (nm)[a]	PDI	Zeta potential (mV)[a]
MSNs	167.27 ± 0.19	0.031	−24.40 ± 0.28
M(a)D	182.03 ± 0.62	0.056	−18.93 ± 0.19
M(a)D@PI	210.23 ± 1.70	0.083	−26.60 ± 0.22
M(a)D@PI-PEG	227.20 ± 1.02	0.125	−24.37 ± 0.09
M(a)D@PI-PEG-RGD	297.60 ± 0.43	0.213	−13.30 ± 0.14

[a]Data represented as mean ± SD, $n = 3$.

Aside from testing for photothermal effect, ROS generation capability was also detected by DPBF. Different formulations were mixed with DPBF and then treated with laser irradiation (1 W/cm^2, 808 nm) for 5 min. The absorbance changes of different formulations were recorded within 5 min. The absorbances of ICG, M(a)D@PI, M(a)D@PI-PEG decreased significantly which demonstrated that nanoparticles can generate ROS according to Fig. 1D. However, the absorbances of DPBF and M(a)D@P had no change, indicating that photodynamic effect was performed by ICG.

3.3. *In vitro drug cumulative release evaluation*

The drug release capability of M(a)D@PI-PEG was detected under various conditions (pH 5.5, pH 5.5 with laser, pH 7.4 and pH 7.4 with laser). We could find that the nanoparticles had pH-responsive performance. M(a)D@PI-PEG exhibited a higher DOX release at pH 5.5 than nanoparticles at pH 7.4. The accumulative DOX release of nanoparticles could reach 21.76% at pH 5.5; however, the accumulative release of DOX from nanoparticles could only reach 13.87% at pH 7.4 (Fig. 2B). It demonstrated that PDA could restrain DOX release at normal environment and reduce drugs leakage before arriving at tumor sites. DOX loaded into nanoparticles can release continually for a long time. While NH_4HCO_3 can transform CO_2 bubbles which could destroy PDA surface, making DOX release more easily. Nanoparticles with laser irradiation can cause hyperthermia which made temperature increase in a short time, potentially inducing transformation of NH_4HCO_3. At the same time, acidic environment at tumor sites also played a vital role in decomposition of NH_4HCO_3. The accumulative DOX release of nanoparticles with laser was higher than nanoparticles without laser at pH 7.4 or 5.5. It indicated that NH_4HCO_3 can accelerate DOX release. DOX release curves of M(a)D is shown as Supporting Information Fig. S6. M(a)D exhibited a higher drug accumulate release with 41.53% at pH 7.4 and 68.50% at pH 5.5 than M(a)D@PI-PEG. It indicates that PDA layer can block DOX in pores of MSNs and suppressed drug release.

3.4. *In vitro cytotoxicity study*

Survival rates of CT26 cells treated with different formulations were evaluated by MTS assay. These results are shown in Fig. 3 and Supporting Information Fig. S7. As shown in Fig. S7B, the nanoparticles displayed low toxic. The results indicate that the cell survival rates cultured with different formulations [DOX, M(a)D@P-PEG, M(a)D@P-PEG-RGD] decreased with the increased DOX concentration according to Fig. 3A, which shows a clear DOX concentration-dependent cytotoxic effect. Furthermore, free DOX displayed better in anti-tumor cells *in vitro* than in nanoparticles. For example, the cell survival (72 h, 8 μg/mL) was 6.49% for free DOX, 11.30% for M(a)D@PI-PEG and 10.40% for M(a)D@PI-PEG-RGD. This is because free DOX can easily enter the cells and nucleus through passive diffusion, inducing undesirable side effects. DOX loaded into nanoparticles can solve these problems and improve *in vivo* biodistribution and bioavailability. Since only a part of DOX could release from the carriers and came into tumor cells to restrain tumor cells growth, the nanoparticles showed a lower cytotoxic effect. Compared the results between Fig. S7A and Fig. 3A, the survival of cells treated with DOX shows no obvious change between 48 and 72 h. At 48 h, the survival of cells treated with DOX was much obvious than that of cells treated with nanoparticles. However, at 72 h, the survival of cells treated with nanoparticles decreased significantly resulting from drug release. Meanwhile, there were significant differences between nanoparticles with laser and without laser (Fig. 3B), which could be explained that both the photothermal effect and photodynamic effect played important roles in cells. Additionally, cells cultured with free ICG + laser only showed a high cell survival. That is because free ICG had low stability and suffered from photo-bleaching, so photothermal and photodynamic effect were not significant. This indicates that ICG displayed better stability after being loaded onto nanoparticles, as well as caused the temperature to rise and generated ROS more effectively.

3.5. *In vitro cellular uptake evaluation*

CT26 cells incubated with different formulations were observed under CLSM (Fig. 4). The results demonstrated that ICG fluorescence of nanoparticles and free ICG mainly distributed in cytoplasm. It showed that the ICG fluorescence of M(a)D@PI-PEG-RGD with laser irradiation was strongest compared with other formulations. From the flow cytometry results (Supporting Information Fig. S8), it can be found that M(a)D@PI-PEG-RGD was easier to enter intercellular environment with the assistance of targeting effect and laser irradiation. Meanwhile, DOX fluorescence of nanoparticles can also be discovered under CLSM. This can explain that cells can take up nanoparticles *via* endocytosis and DOX can be released under stimulation. However, the DOX fluorescence signal of free DOX indicates that most free DOX entered nucleus but the DOX fluorescence of DOX loaded into nanoparticles mostly distributed in the cytoplasm and these signals in nucleus was relative weaker, which can be explained that part of DOX could release from nanoparticles. Next, CT26 cells were pretreated with excess RGD to demonstrate receptor mediated endocytosis for M(a)D@PI-PEG-RGD.

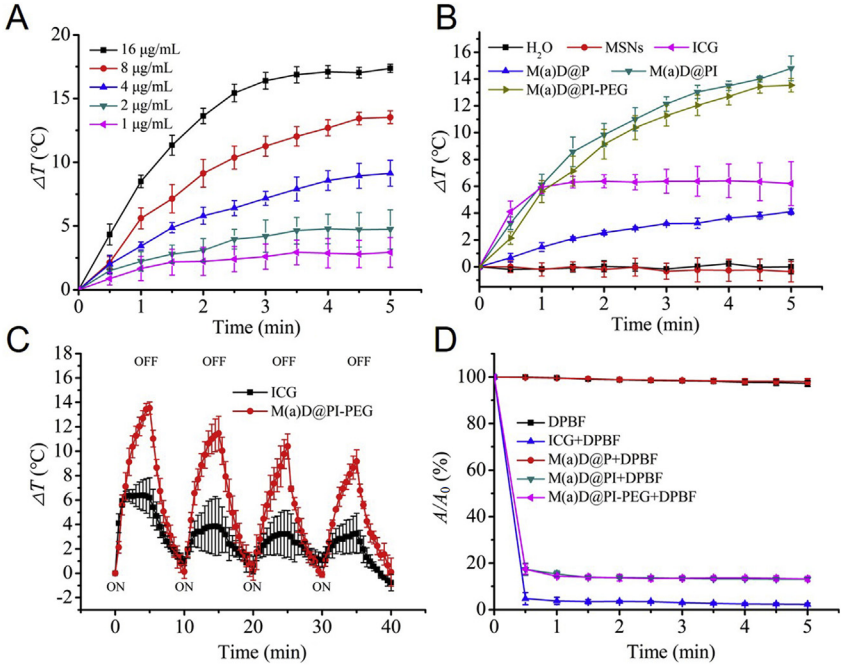

Figure 1 Photothermal effect and ROS detection of different formulations *in vitro*. (A) Temperature changes of different ICG equivalent concentrations for M(a)D@PI-PEG treated with laser irradiation (1 W/cm^2, 808 nm, 5 min). (B) Temperature changes of different formulations treated with laser irradiation (1 W/cm^2, 808 nm, 5 min) with same ICG equivalent concentration (8 μg/mL). (C) Temperature changes of free ICG and M(a)D@PI-PEG with same ICG equivalent concentration (8 μg/mL) treated with laser irradiation (1 W/cm^2, 808 nm, 5 min) over four laser ON/OFF cycles. (D) Change of UV absorbance values at 410 nm for different formulations treated with laser irradiation (1 W/cm^2, 808 nm, 5 min). All data represented as mean ± SD (n = 3).

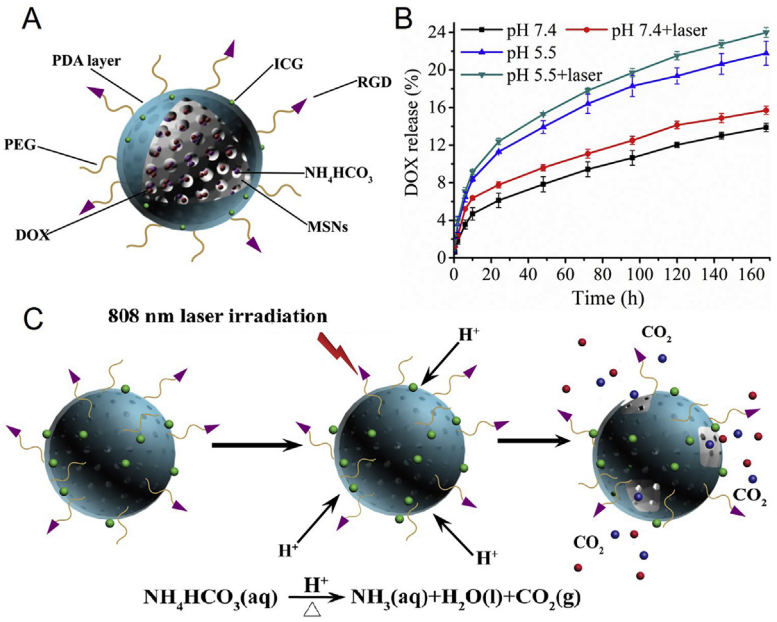

Figure 2 The schematic illustration and characterization of drug release. (A) Structure illustration of M(a)D@PI-PEG-RGD. (B) DOX release curves of M(a)D@PI-PEG at different medium, the data were shown as mean ± SD ($n = 3$). (C) The illustration of NH_4HCO_3 transformed into CO_2 bubbles and destroyed PDA layer.

The result is shown as Supporting Information Fig. S9. The intracellular fluorescence of cells pretreated with RGD decreased obviously, showing that cellular uptake was partly inhibited resulting from the fact that free RGD would occupy the receptors on the surfaces of cell.

3.6. *In vitro ROS detection and analysis*

Carboxy-H_2DCFDA was used as a ROS-sensitive probe to detect ROS and cells were observed under CLSM and the results are shown as Fig. 5. Combined with flow cytometry results (Supporting Information Fig. S10), it indicates that nanoparticles can generate more ROS with the stimulation of laser irradiation compared with free ICG resulting from higher cell internalization. Due to the low stability of ICG, free ICG can only generate a small amount of ROS even treated with laser irradiation. M(a)D@PI-PEG-RGD could generate most ROS compared with other formulations. Based on these findings, the targeting effect was evident.

3.7. *Imaging in vivo and biodistribution study*

To explore the drugs and nanoparticles distribution *in vivo*, different mice groups were treated with different formulations and then observed under Imaging System *in vivo* (CRi Maestro™). As shown in Fig. 6A, free drugs and nanoparticles could be delivered to tumor sites. The ICG fluorescence signals of different groups were strongest after 12 h of injection. The ICG fluorescence became gradually weaker after 24, 48 and 72 h of injection. Combined with the results of Fig. 6C, the ICG fluorescence at tumor sites of mice injected with M(a)D@PI-PEG-RGD appeared strongest, compared with that of the free ICG + DOX and M(a)D@PI-PEG at the same time points. These results demonstrate that targeting effect was also favorable *in vivo* and nanoparticles can arrive at tumor sites more easily than free drugs. On 72 h, ICG fluorescence of group treated with ICG + DOX almost disappeared while the ICG fluorescence of group treated with nanoparticles was still present. It indicates that nanoparticles were stable and can extend drug circulation time in blood.

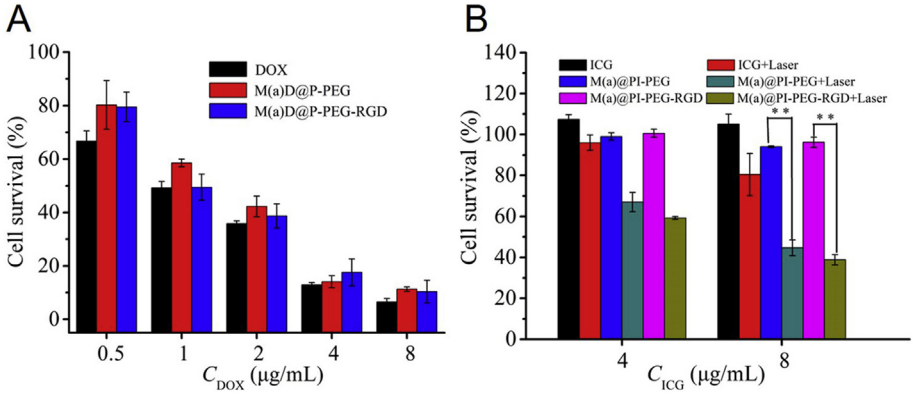

Figure 3 The cytotoxicity of different formulations (A) Survival of CT26 treated with various formulations at different DOX concentrations (B) Survival of CT26 treated with various formulations at different ICG concentrations. Some groups were treated with laser irradiation (1 W/cm^2, 808 nm, 5 min). All data represented as mean ± SD ($n = 3$), *$P < 0.05$, **$P < 0.01$.

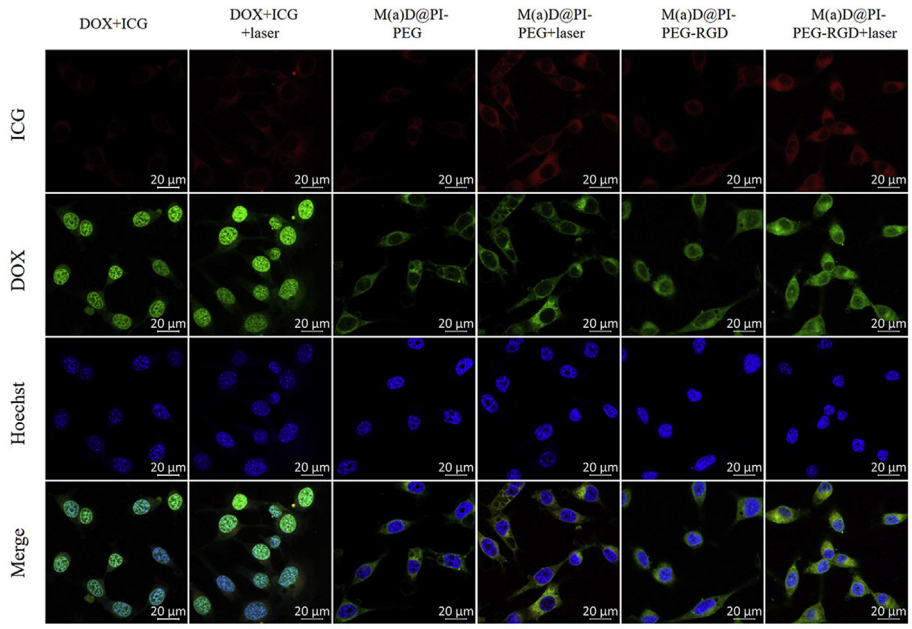

Figure 4 CLSM images of CT26 cells incubated with various formulations, scale bar = 20 μm; Laser: 1 W/cm^2, 808 nm, 5 min.

At the same time, *ex vivo* images of hearts, livers, spleens, lungs, kidneys and tumors can also support above conclusions (Fig. 6B).

The result for distribution of M(a)D@PI-PEG-RGD in organs is shown in Supporting information Fig. S11. At 12 h, nanoparticles can accumulate abundantly in tumor sites (37.1 μg/g). Nanoparticles can also accumulate in other organs (42.3, 25.8, 32.5, 44.4 and 18.6 μg/g for heart, liver, spleen, lung and kidney, respectively). However, nanoparticles accumulations in organs decreased at 72 h. The result shows that nanoparticles will not accumulate abundantly in main organs.

3.8. *In vivo photothermal effect study*

After 12 h of injection, different groups were irradiated with 808 nm laser (1 W/cm^2) for 5 min. The temperatures from each condition were recorded. From Fig. 7A, it was found that the temperature of mice tumor site treated with M(a)D@PI-PEG-RGD increased rapidly over 50 °C, which can cause protein denaturation, cellular disruption as well as tumor cell apoptosis. The group treated with M(a)D@PI-PEG can rise to 45.8 °C, which was also high enough to cause irreversible damage to tumor cells. At the same time, group treated with free ICG + DOX did not show an obvious photothermal effect because of poor stability. It confirmed that nanoparticles can effectively cause irreversible damage to tumor cells with the assistance of photothermal effect.

3.9. *In vivo ROS detection and tunnel apoptotic cell detection of tumor tissues evaluation*

Several tumor sites slices were dealt and observed under CLSM. As shown in Fig. 8A, tumor sites treated with M(a)D@PI-PEG + laser and M(a)D@PI-PEG-RGD + laser showed strong green fluorescence signals which indicated that a large variety of ROS had generated. Tumor sites treated with targeting modified

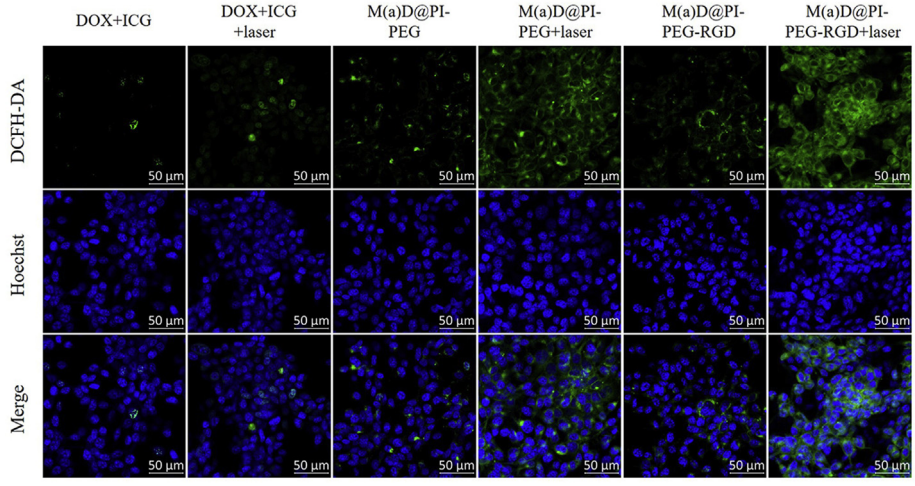

Figure 5 CLSM images of CT26 cells incubated with various formulations for ROS detection, scale bar = 50 μm; Laser: 1 W/cm^2, 808 nm, 5 min.

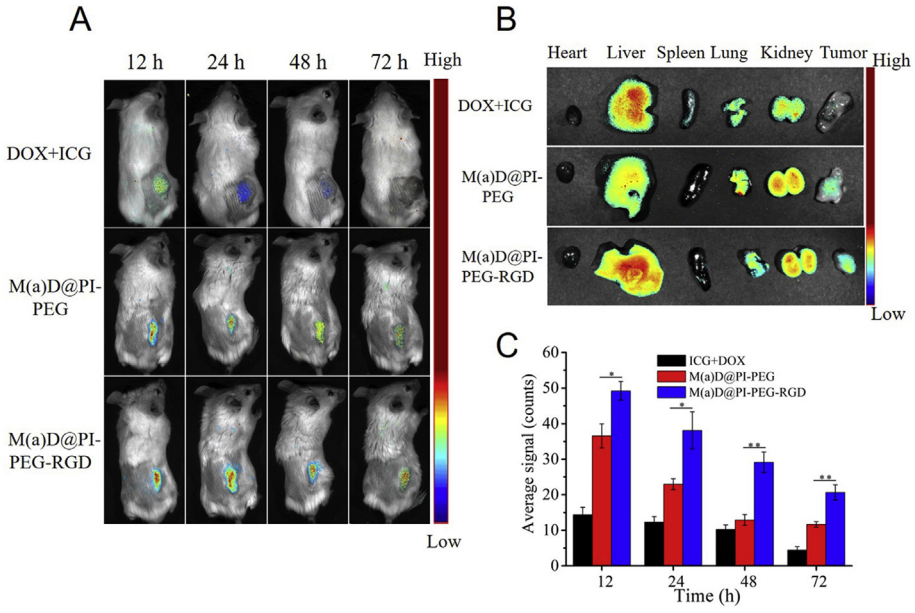

Figure 6 Near-infrared images of CT26 tumor bearing BALB/c female mice after injection *via* tail of free DOX + ICG, M(a)D@PI-PEG and M(a)D@PI-PEG-RGD (at DOX dosage of 8 mg/kg, at ICG dosage of 1.36 mg/kg). (A) ICG fluorescence images from various groups at different time points *in vivo*. (B) *Ex vivo* DOX fluorescence images for major organs and tumors at 12 h after injection. (C) Semi-quantitative evaluation of ICG fluorescence intensity for tumor sites. All data represented as mean ± SD ($n = 3$). *$P < 0.05$, **$P < 0.01$.

nanoparticles generated more ROS than that of M(a)D@PI-PEG. Free drugs generated least ROS compared with nanoparticles. ICG loaded onto nanoparticles can play a more important role than free ICG + DOX. ROS can result in irreversible damage of tumor sites and kill tumor effectively. According to these results, we found that nanoparticles were highly desirable for PTT and PDT.

These mice were sacrificed, tumors sites were collected and preserved in 4% paraformaldehyde and dehydrated, then cut into slices. At last these slices were dealt with antifade mounting medium containing DAPI, and then observed *via* CLSM (Fig. 8B). Green fluorescence signals represented the apoptotic cell nucleus while blue fluorescence signals represented normal cell nucleus in tumor sites. It indicates that M(a)D@PI-PEG-RGD + laser can make more cells in tumor sites undergo apoptosis compared with other three groups. Nanoparticles had an outstanding ability to kill tumor cells according to results above. Combination therapy was remarkable when performed by nanoparticles.

3.10. *Therapeutic efficacy study*

The experiment lasted 14 days and tumor volume change curve is shown as Fig. 9B. At the end, the mice tumor growths treated with nanoparticles and free drugs were all constrained and tumor volumes at the last day were 281 mm^3 for ICG + DOX + laser, 183 mm^3 for M(a)D@PI-PEG + laser, 509 mm^3 for M(a)D@PI-PEG-RGD and 76 mm^3 for M(a)D@PI-PEG-RGD + laser, respectively. However, the mice tumor volume treated with PBS grew rapidly and reached

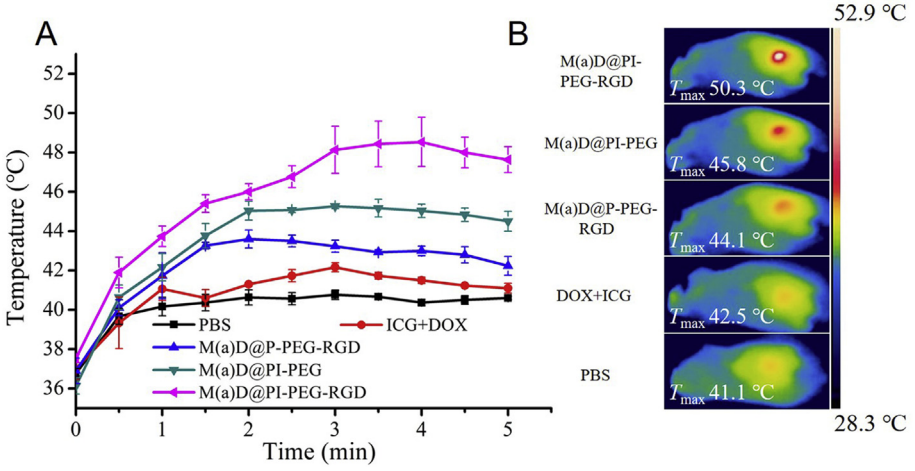

Figure 7 Photothermal response *in vivo*. (A) Temperature curves for tumor sites of mice injected with different formulations under laser irradiation (1 W/cm^2, 808 nm, 5 min). All data represented as mean ± SD ($n = 3$). (B) The max temperature images for tumor sites of mice injected with different formulations under irradiation (1 W/cm^2, 808 nm, 5 min).

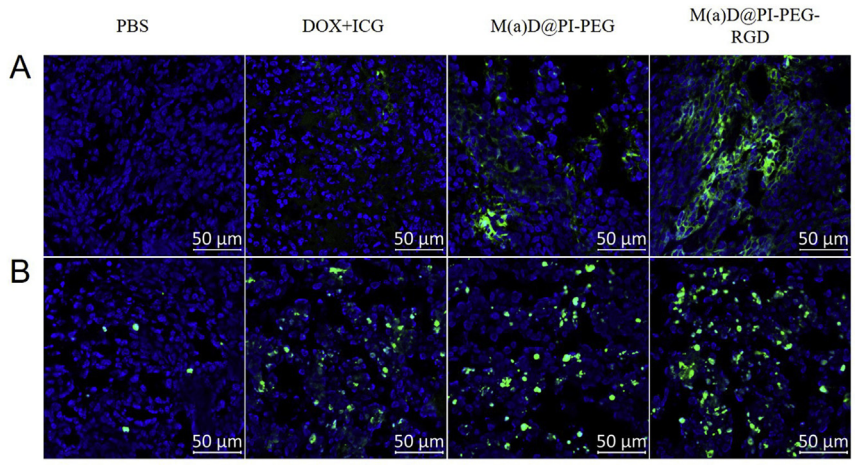

Figure 8 ROS and tunnel apoptotic cell detection of tumor tissues. (A) CLSM images for tumor sites of mice treated with different formulations under laser irradiation (1 W/cm^2, 808 nm, 5 min) for ROS detection. (B) Images of tunnel apoptotic cell detection for tumor tissues of mice treated with different formulations under irradiation (1 W/cm^2, 808 nm, 5 min). Scale bar = 50 μm.

1227 mm^3 within 14 days. It demonstrates that chemotherapy performed by M(a)D@PI-PEG-RGD and combination therapy performed by ICG + DOX + laser as well as nanoparticles + laser were both effective to suppress tumor growth. Compared with the free drugs-treated mice, tumor volumes of mice treated with M(a)D@PI-PEG-RGD + laser and M(a)D@PI-PEG + laser at last day were much smaller. Accordingly, we can deduce that the combination therapy of free drug was not more effective than that of nanoparticles, which resulted from poor accumulation and instability of drugs in tumor. After modifying RGD, therapeutic effect was enhanced because of targeting effect through comparing the group treated with M(a)D@PI-PEG-RGD + laser and that of M(a)D@PI-PEG + laser. Targeting modification played an essential role in the nanoparticles' accumulation in tumor sites. The tumor growth of the group treated with M(a)D@PI-PEG-RGD still can be restrained but is not effective than that of M(a)D@PI-PEG-RGD + laser. It is shown that chemotherapy was not as effective as combination therapy. The excellent antitumor effect of M(a)D@PI-PEG-RGD contributed to the stability of nanoparticles *in vivo*, DOX and ICG can accumulate in tumor sites *via* targeting and EPR effect. Additionally, laser irradiation can cause local hyperthermia and ROS-generation which can achieve synergistic therapeutic effects with chemotherapy to inhibit tumor growth. The body weight change is an important parameter for analyzing toxicity and biocompatibility. Body weight change curves indicate no significant body change for the groups treated with nanoparticles, showing nanoparticles had good biocompatibility and

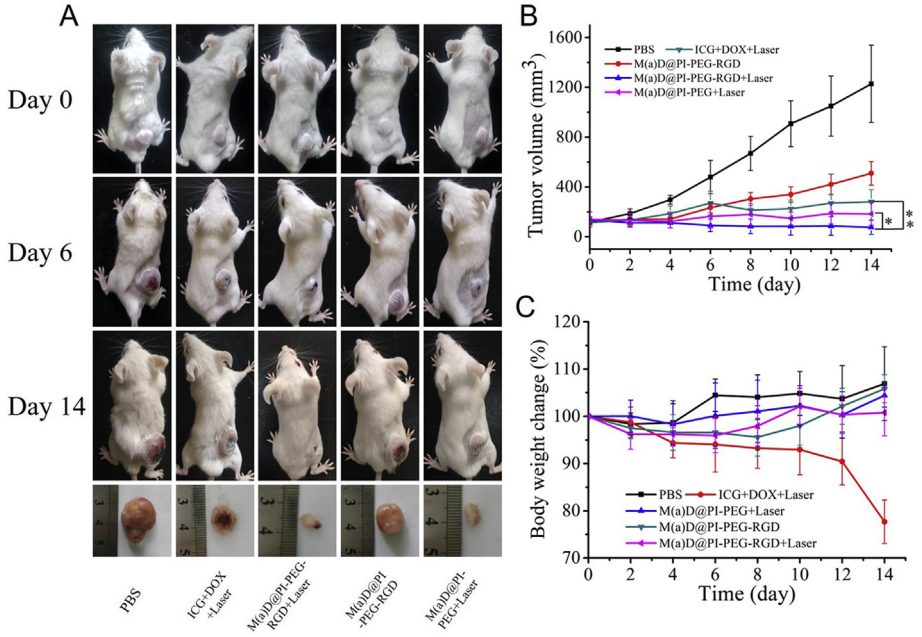

Figure 9 *In vivo* combination therapy effect. (A) Photos of BALB/c mice bearing CT26 tumors at different time points and tumor issues images on 14 day. (B) Tumor volume curves of mice treated with different formulations. (C) Body weight change curves of mice treated with different formulations. The data were shown as mean ± SD ($n = 6$), *$P < 0.05$, **$P < 0.01$.

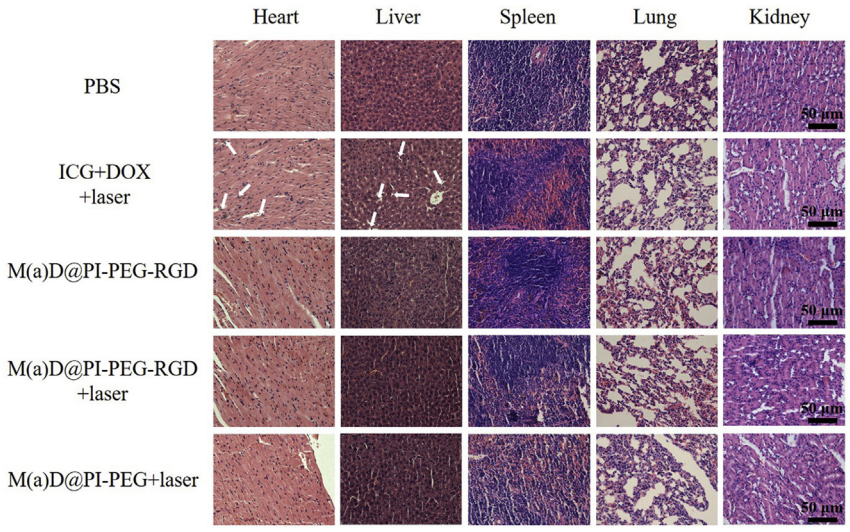

Figure 10 H&E staining for major organs from mice treated with different formulations after 14 days, scale bar = 50 μm.

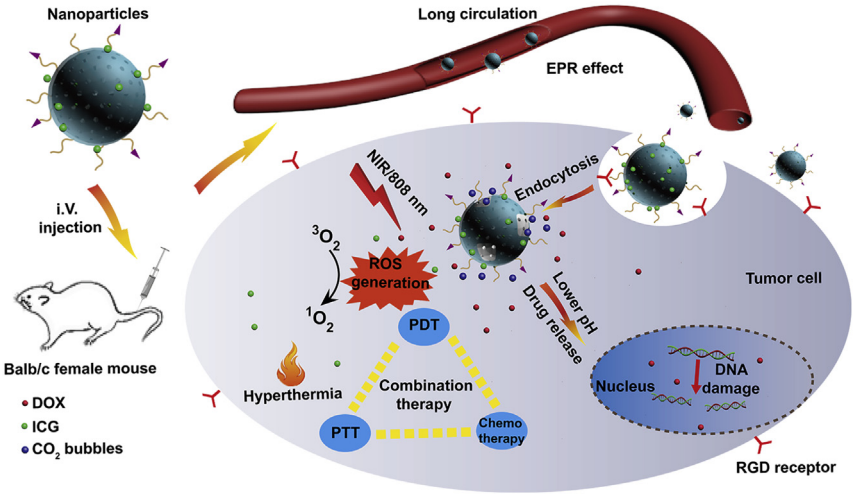

Scheme 1 Schematic illustration of pH-sensitive and bubble-generating mesoporous silica-based nanoparticles for enhanced tumor combination therapy.

low toxicity. But the body weight changed obviously for the group treated with free drugs. This is related to the toxicity and the non-specificity of drugs.

3.11. Histological analysis

The therapy influence of free drugs and nanoparticles was further analyzed by H&E staining (Fig. 10). The results indicate that the major organs of mice treated with nanoparticles and PBS showed no obvious tissue damage. Meanwhile, we found necrosis in the tissues of mice heart and liver treated with free drugs. The nanoparticles are confirmed to attenuate side effects of anti-tumor drugs effectively.

4. Conclusions

In our study, a new system of nanoparticles has been successfully synthesized with RGD-functionalization and PDA-modification. The nanoparticles could be delivered to tumor sites through RGD targeting effect. We endowed nanoparticles with PTT, PDT, and chemotherapy to enhance anti-tumor effect. Temperature changes and ROS generation of nanoparticles were obvious under NIR irradiation *in vitro* and *vivo*. The NH_4HCO_3-loaded into nanoparticles could accelerate DOX release to enhance chemotherapy effect. The results of animal experiments show that M(a)D@PI-PEG-RGD + laser had an outstanding anti-tumor effect. Thus, the pH-sensitive and bubble-generating mesoporous silica-based nanoparticles would be a promising system for nano-drug delivery and tumor combination therapy.

Acknowledgments

This work was supported by National Natural Science Foundation of China (Nos. 81671806 and 81571793); Chinese Academy of Medical Science Initiative for Innovative Medicine (Nos. 2017-I2M-4-001 and 2017-I2M-3-020, China); Fundamental Research Funds for the Central Universities (Nos. 2019PT320028, 2019-0831-03 and 3332019100, China).

Author contributions

Dunwan Zhu and Linhua Zhang conceived and designed this research. Zhiming Zhang and Chenlu Huang carried out the experiments. Zhiming Zhang wrote the manuscript. Li Zhang, Qing Guo, Yu Qin and Fan Fan participated part of the experiments. Bao Xiao performed part of the characterizations. Boxuan Li revised the manuscript. All of the authors have read and approved the final manuscript.

Conflicts of interest

The authors have no conflicts of interest to declare.

Appendix A. Supporting information

Supporting data to this article can be found online at https://doi.org/10.1016/j.apsb.2020.08.013.

References

1. Li J, Li Y, Wang Y, Ke W, Chen W, Wang W, et al. Polymer prodrug-based nanoreactors activated by tumor acidity for orchestrated oxidation/chemotherapy. *Nano Lett* 2017;**11**:6983−90.
2. Wang JL, Du XJ, Yang JX, Shen S, Li HJ, Luo YL, et al. The effect of surface poly(ethylene glycol) length on *in vivo* drug delivery behaviors of polymeric nanoparticles. *Biomaterials* 2018:104−13.
3. Han Y, Ding B, Zhao Z, Zhang H, Sun B, Zhao Y, et al. Immune lipoprotein nanostructures inspired relay drug delivery for amplifying antitumor efficiency. *Biomaterials* 2018:205−18.
4. Gao Y, Chen Y, Ji X, He X, Yin Q, Zhang Z, et al. Controlled intracellular release of doxorubicin in multidrug-resistant cancer cells by tuning the shell-pore sizes of mesoporous silica nanoparticles. *ACS Nano* 2011;**12**:9788−98.
5. Yang Y, Guo Q, Peng J, Su J, Lu X, Zhao Y, et al. Doxorubicin-conjugated heparin-coated superparamagnetic iron oxide nanoparticles for combined anticancer drug delivery and magnetic resonance imaging. *J Biomed Nanotechnol* 2016;**11**:1963−74.
6. Gupta B, Poudel BK, Ruttala HB, Regmi S, Pathak S, Gautam M, et al. Hyaluronic acid-capped compact silica-supported mesoporous titania nanoparticles for ligand-directed delivery of doxorubicin. *Acta Biomater* 2018:364−77.
7. Gao Y, Yang C, Liu X, Ma R, Kong D, Shi L. A multifunctional nanocarrier based on nanogated mesoporous silica for enhanced tumor-specific uptake and intracellular delivery. *Macromol Biosci* 2012;**2**:251−9.
8. Gao W, Hu Y, Xu L, Liu M, Wu H, He B. Dual pH and glucose sensitive gel gated mesoporous silica nanoparticles for drug delivery. *Chin Chem Lett* 2018;**29**:107−10.
9. Zhou Y, Quan G, Wu Q, Zhang X, Niu B, Wu B, et al. Mesoporous silica nanoparticles for drug and gene delivery. *Acta Pharm Sin B* 2018;**2**:165−77.
10. Zhu D, Fan F, Huang C, Zhang Z, Qin Y, Lu L, et al. Bubble-generating polymersomes loaded with both indocyanine green and doxorubicin for effective chemotherapy combined with photothermal therapy. *Acta Biomater* 2018:386−97.
11. Yu M, Guo F, Tan F, Li N. Dual-targeting nanocarrier system based on thermosensitive liposomes and gold nanorods for cancer thermo-chemotherapy. *J Control Release* 2015:91−100.
12. Chen KJ, Liang HF, Chen HL, Wang Y, Cheng PY, Liu HL, et al. A thermoresponsive bubble-generating liposomal system for triggering localized extracellular drug delivery. *ACS Nano* 2013;**1**:438−46.
13. Wei Y, Gao L, Wang L, Shi L, Wei E, Zhou B, et al. Polydopamine and peptide decorated doxorubicin-loaded mesoporous silica nanoparticles as a targeted drug delivery system for bladder cancer therapy. *Drug Deliv* 2017;**1**:681−91.
14. Hu D, Liu C, Song L, Cui H, Gao G, Liu P, et al. Indocyanine green-loaded polydopamine-iron ions coordination nanoparticles for photoacoustic/magnetic resonance dual-modal imaging-guided cancer photothermal therapy. *Nanoscale* 2016;**39**:17150−8.
15. Hu D, Zhang J, Gao G, Sheng Z, Cui H, Cai L. Indocyanine green-loaded polydopamine-reduced graphene oxide nanocomposites with amplifying photoacoustic and photothermal effects for cancer theranostics. *Theranostics* 2016;**7**:1043−52.
16. Xue P, Hou M, Sun L, Li Q, Zhang L, Xu Z, et al. Calcium-carbonate packaging magnetic polydopamine nanoparticles loaded with indocyanine green for near-infrared induced photothermal/photodynamic therapy. *Acta Biomater* 2018:242−55.
17. Pang X, Jiang Y, Xiao Q, Leung AW, Hua H, Xu C. pH-Responsive polymer-drug conjugates: design and progress. *J Control Release* 2016:116−29.
18. Ren S, Cheng X, Chen M, Liu C, Zhao P, Huang W, et al. Hypotoxic and rapidly metabolic PEG-PCL-C3-ICG nanoparticles for fluorescence-guided photothermal/photodynamic therapy against OSCC. *ACS Appl Mater Interfaces* 2017;**37**:31509−18.
19. Zhu H, Cheng P, Chen P, Pu K. Recent progress in the development of near-infrared organic photothermal and photodynamic nanotherapeutics. *Biomater Sci* 2018;**4**:746−65.
20. Hu H, Xiao C, Wu H, Li Y, Zhou Q, Tang Y, et al. Nanocolloidosomes with selective drug release for active tumor-targeted imaging-guided photothermal/chemo combination therapy. *ACS Appl Mater Interfaces* 2017;**48**:42225−38.
21. Zhang H, Zhang X, Zhu X, Chen J, Chen Q, Zhang H, et al. NIR light-induced tumor phototherapy using photo-stable ICG delivery system based on inorganic hybrid. *Nanomedicine* 2018;**1**:73−84.
22. Guo X, Qu J, Zhu C, Li W, Luo L, Yang J, et al. Synchronous delivery of oxygen and photosensitizer for alleviation of hypoxia tumor microenvironment and dramatically enhanced photodynamic therapy. *Drug Deliv* 2018;**1**:585−99.
23. Yang Y, Zhu W, Feng L, Chao Y, Yi X, Dong Z, et al. G-quadruplex-based nanoscale coordination polymers to modulate tumor hypoxia and achieve nuclear-targeted drug delivery for enhanced photodynamic therapy. *Nano Lett* 2018;**11**:6867−75.
24. Lee YH, Chang DS. Fabrication, characterization, and biological evaluation of anti-HER2 indocyanine green-doxorubicin-encapsulated PEG-*b*-PLGA copolymeric nanoparticles for targeted photochemotherapy of breast cancer cells. *Sci Rep* 2017:46688.
25. Pan L, He Q, Liu J, Chen Y, Ma M, Zhang L, et al. Nuclear-targeted drug delivery of TAT peptide-conjugated monodisperse mesoporous silica nanoparticles. *J Am Chem Soc* 2012;**13**:5722−5.
26. Schmid D, Park CG, Hartl CA, Subedi N, Cartwright AN, Puerto RB, et al. T cell-targeting nanoparticles focus delivery of immunotherapy to improve antitumor immunity. *Nat Commun* 2017;**1**:1747.
27. Zhang L, Qin Y, Zhang Z, Fan F, Huang C, Lu L, et al. Dual pH/reduction-responsive hybrid polymeric micelles for targeted chemo-photothermal combination therapy. *Acta Biomater* 2018:371−85.
28. Zhu D, Tao W, Zhang H, Liu G, Wang T, Zhang L, et al. Docetaxel (DTX)-loaded polydopamine-modified TPGS-PLA nanoparticles as a targeted drug delivery system for the treatment of liver cancer. *Acta Biomater* 2016:144−54.
29. Liang G, Jin X, Zhang S, Xing D. RGD peptide-modified fluorescent gold nanoclusters as highly efficient tumor-targeted radiotherapy sensitizers. *Biomaterials* 2017:95−104.
30. Zhou A, Wei Y, Chen Q, Xing D. *In vivo* near-infrared photodynamic therapy based on targeted upconversion nanoparticles. *J Biomed Nanotechnol* 2015;**11**:2003−10.

31. Zhang N, Li C, Zhou D, Ding C, Jin Y, Tian Q, et al. Cyclic RGD functionalized liposomes encapsulating urokinase for thrombolysis. *Acta Biomater* 2018:227−36.
32. Villa CH, McDevitt MR, Escorcia FE, Rey DA, Bergkvist M, Batt CA, et al. Synthesis and biodistribution of oligonucleotide-functionalized, tumor-targetable carbon nanotubes. *Nano Lett* 2008;**12**:4221−8.
33. Yan J, Zhang H, Cheng F, He Y, Su T, Zhang X, et al. Highly stable RGD/disulfide bridge-bearing star-shaped biodegradable nanocarriers for enhancing drug-loading efficiency, rapid cellular uptake, and on-demand cargo release. *Int J Nanomed* 2018:8247−68.
34. Jiang K, Shen M, Xu W. Arginine, glycine, aspartic acid peptide-modified paclitaxel and curcumin co-loaded liposome for the treatment of lung cancer: *in vitro/vivo* evaluation. *Int J Nanomed* 2018: 2561−9.
35. Win KY, Feng SS. Effects of particle size and surface coating on cellular uptake of polymeric nanoparticles for oral delivery of anticancer drugs. *Biomaterials* 2005;**15**:2713−22.
36. Saxena V, Sadoqi M, Shao J. Indocyanine green-loaded biodegradable nanoparticles: preparation, physicochemical characterization and *in vitro* release. *Int J Pharm* 2004;**2**:293−301.